Title
A mini review of cobalt-based nanocatalyst in Fischer-Tropsch synthesis

Authors
Qi, Zhiyuan
Chen, Luning
Zhang, Shuchen
et al.

Publication Date
2020-07-01

DOI
10.1016/j.apcata.2020.117701

Peer reviewed

A Mini Review of Cobalt-based Nanocatalyst in Fischer-Tropsch Synthesis

Zhiyuan Qi[1], Luning Chen[2], Shuchen Zhang[2], Ji Su[2,3], Gabor A. Somorjai[2,4]

[1] Chemical Sciences Division,

[2] Materials Sciences Division,

[3] Molecular Foundry, Lawrence Berkeley National Laboratory, Berkeley, CA, 94720, United States

[4] Department of Chemistry, University of California-Berkeley, Berkeley, CA, 94720, United States

Correspondence: jisu@lbl.gov (Ji Su);
somorjai@berkeley.edu (Gabor A. Somorjai)

Graphical abstract

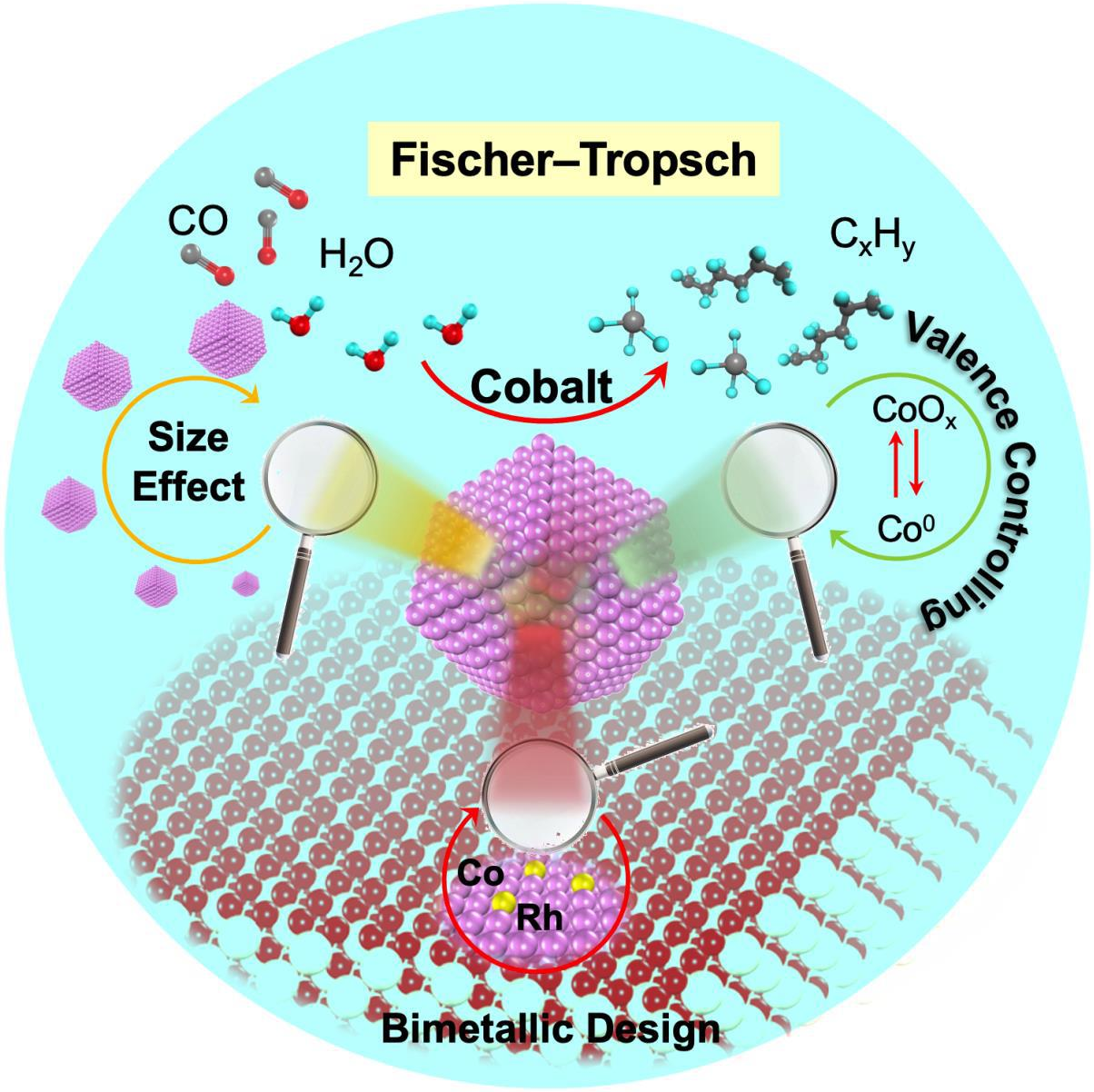

Highlights

- Convert syngas to paraffin and alcohols catalyzed by Co-based catalysts
- Size and support dependence of Co catalysts on Fischer-Tropsch synthesis
- Product distribution controlled by the surface compositions
- Chemical transient kinetics experiments to study the non-steady state chemistry

Abstract

Fischer-Tropsch (F-T) synthesis, converting syngas to hydrocarbons, provides a green alternative for fuel production. Cobalt is one of the most intensively studied F-T catalysts due to its great activity, high stability, and relatively low cost. In this mini review, we summarized some recent advancements in the development of cobalt-based F-T catalysts focusing on the effects of particle size, surface oxidation states, crystallography, and bimetallic particles, with emphasis on the research from our group. Furthermore, non-steady state conditions were investigated to access the initial kinetics using chemical transient kinetics (CTK) experiments, which could bring more insights into the reaction mechanism and catalysis design.

Keywords : Fischer-Tropsch synthesis, Chemical transient kinetics, Cobalt catalysis, Structure-property relationship

Contents

1 Introduction

Synthesis gas or syngas, a mixture of hydrogen and carbon monoxide, has been used in the industry as a source of fuels and chemicals[1]. The production of syngas is well established, including steam reforming of natural gas[2], gasification of coals[3], conversion of biomass and other organic wastes[4].

$$CH_4 + H_2O \xrightarrow[750-900\,^{\circ}C]{nickele\ catalyst} 3H_2 + CO \qquad \text{(Steam methane reforming reaction)}$$

Depending on the production method and the raw materials (especially the carbon to hydrogen ratios), the chemical composition of syngas varies widely. However, syngas can still work as the source of pure hydrogen. The CO in the synthesis gas can yield another molecular H_2 via water-gas shift reaction, where the pure H_2 can be obtained after removing CO_2 and used in the synthesis of ammonia, hydrogen peroxide, methanol and other fine chemicals[5]. Pure carbon monoxide can be obtained by cryogenic separation or absorption in aqueous copper salt solutions[5].

$$CO + H_2O \rightarrow CO_2 + H_2 \qquad \text{(Water gas shift reaction)}$$

Besides as the hydrogen and CO source, syngas is also used for electricity generation[6], synthesis of methanol[7-9], and directly as a fuel[10]. Among all applications of syngas, Fischer-Tropsch (F-T) synthesis is a crucial reaction that produces hydrocarbons ranging from CH_4 to long carbon chains such as gasoline and diesel. Sabatier et al. first reported the hydrogenation of CO to form methane in 1902[11]. Fischer and Tropsch then discovered "gasoline synthesis" from CO and H_2 in 1926. F-T synthesis usually produces a mixture of hydrocarbons with different carbon numbers via a multi-step reaction. As shown in the equation (1), -CH_2 intermediates are formed to achieve chain growth, leading to the production of paraffin or olefins. The growth of carbon chains requires breaking the C-O band, the addition of hydrogen atoms to carbon and oxygen, and forming a new C-C bond. It is widely accepted that the formation of one -CH_2 intermediate group involves 1) associative adsorption of CO; 2) splitting the C-O bond; 3) dissociative adsorption of two H_2 molecules; 4) water formation; 5) water desorption; 6) (CH_2) formation by transfer another two H

atoms to the carbon atom. Therefore, the formation of metal carbonyls on the surface is believed to be crucial to produce hydrocarbons. A more detailed mechanism was summarized in the review by Schulz[12].

$$CO + 2H_2 \rightarrow (CH_2) + H_2O \quad (1)$$

$$(2n+1)H_2 + nCO \rightarrow C_nH_{2n+2} + nH_2O \quad (2)$$

$$(2n)H_2 + nCO \rightarrow C_nH_{2n} + nH_2O \quad (3)$$

2 Fischer-Tropsch catalyst

F-T catalysts usually are (1) active for hydrogenation reactions; (2) capable to form metal carbonyl around the F-T reaction conditions[12]. Iron and cobalt are the traditional catalysts for "gasoline synthesis", and are still used for industrial application[13]. Nickel, ruthenium and rhodium are also typical F-T catalysts. Nickel selectively produces methane at higher temperatures and forms volatile "surface carbonyl" at elevated pressure, causing the deactivation and continuous loss of metal under commercial reaction conditions[14]. Thus, nickel has not been commercialized for the F-T process[14, 15]. Ruthenium can effectively lower the reaction temperatures due to its high activity and produce long-chain hydrocarbons with high selectivity. However, its industrial application is limited by the scarcity and high-cost. Rhodium-based catalysts have been reported to directly convert syngas to C_{2+} oxygenate due to its moderate adsorption of CO molecules, which will be discussed further in this paper. Both iron and cobalt catalysts have been used for F-T synthesis in the industry. Iron catalysts could selectively produce the linear terminal olefins with the 60-70% selectivity towards C_2-C_4 olefins[16]. It also has activity toward water gas shift reactions, which is favorable for the conversion of CO-rich syngas[17, 18]. However, water as a byproduct will deactivate the iron catalysts via oxidation of the active Fe species and inhibit the rate of FTS. Therefore, it is essential to maintain a low partial pressure of water during industrial operations, usually achieved by the use of reactors in series and removing water from recycled steam[19]. Besides, the activity loss of Fe-based FTS catalysts is also caused by: (1) transition from the active phases (metallic Fe, carbide) to inactive phases (e.g. oxide, inactive carbides); (2) deposition of carbonaceous species on the surface; (3) loss of active sites from sintering; (4) surface poisoning (e.g. sulfur)[20]. Cobalt has gained more attention due to the production of diesel

fuels due its higher activities, higher C_{5+} selectivity, and more resistant to deactivation compared to iron [21]. Re-oxidation of cobalt and formation of poly-carbon are two main reasons for long-term deactivation, while sintering may lead to the loss of activity at the initial stage especially for 6-12 nm crystallites[22]. In addition, carbide formation, poisoning, the formation of stable compounds via interaction between cobalt and supports, surface reconstruction could all cause the deactivation, as summarized in previous reviews[22, 23].

3 Fischer-Tropsch synthesis using Co catalysts

In this mini review, we focused on our recent work on cobalt-based catalysts and summarized the studies of size effect[24], crystallography effect, the influence of surface oxidation state[25] on both pure Co and bimetallic alloys[26]. In addition, chemical transient kinetics (CTK) experiments were discussed including the experimental set-up and the study of reaction under non-steady state condition[27, 28].

3.1 Particle size effect

The synthetic methods of nanoparticles with preciously controlled size and shape were well explored and established since the early 21st centuries, which leads to the rapid growth of nanocatalysis[29]. By using nanomaterials as catalysts, remarkable novel catalytic properties including significantly enhanced activity and selectivity have been reported and new surface chemistry has as well been investigated[30-42]. The activity and selectivity of the F-T process are also size-dependent[37, 38, 42-44]. Early work by Iglesia has reported the turnover frequency (TOF) of F-T synthesis is insensitive to the cobalt particle size over a range of 10-200 nm[45]. However, the TOF will dramatically decrease when the particle size is smaller than 10 nm, and the selectivity to methane increases within smaller nanoparticles[46-48]. The cobalt particle size effect in the range of 2.6-27 nm was investigated by de Jong's group using inert carbon nanofibers as supports. TOF of CO hydrogenation remains almost unchanged when particle sizes are larger than 6 nm (1 bar) or 8 nm (35 bar), but decreased with smaller particle size (< 6 nm)[37].

Our group studied the size effect using cobalt nanoparticles (NPs) with four different sizes (3.2, 5.5, 8.6, and 11 nm) supported by mesoporous silica (MCF-17)[24]. All the catalysts were pretreated in pure oxygen at 350 ˚C, followed by a reduction in hydrogen flow at 450 ˚C. The

reaction was then carried out under a flow of H_2: CO: Ar (2:1:0.08) at 5 bar, with a flow rate of 30 mL/min. Fig.1a shows the increase of CO consumption TOF with increasing particle size at three tested temperatures (190, 220, and 250 ˚C). 11 nm Co NPs shows a 15-fold greater TOF than that fo 3.2 nm Co NPs at 190 ˚C, while only 5-fold enhancement was obtained at 250 ˚C. Moreover, the product distribution is also changed with the particle size (Fig.1b). 11 nm Co has the largest selectivity (~85%) to long-chain products with carbon number higher than 5 (C_{5+}) but the smallest selectivity to methane, while smaller particles are more selective to methane formation (all larger than 30%). This selectivity trend as a function of particle size is consistent with the results reported by de Jong's group[37], while 10 nm Co NPs supported by inert carbon nanofibers exhibited a higher methane selectivity of ~40 wt% and a C_{5+} selectivity of 30 wt%. Zhang and coworkers studied the catalytic performance of Co/Al_2O_3 using different commercial alumina, and a 14.7% methane selectivity and ~80% C_{5+} selectivity were observed on the alumina support with lower acidity[49], which is consistent with some other reports[50, 51]. Therefore, we proposed the high selectivity towards C_{5+} product and low selectivity of undesired methane over 11 nm Co might be explained by the support effect. Besides, the size effect also results in different responses to the temperature changes. Fig.1a demonstrates the increases in TOF with raising temperature for each particle size and Fig.1c-d show the temperature effect on selectivity. At 190 ˚C, all Co NPs with different sizes have very similar selectivity towards methane and C_{5+} product, indicating size effect is not obvious at the lower temperature. However, more methane and less C_{5+} product were formed at a higher temperature in general while temperature effect is more significant on smaller particles, which leads to the large difference in product distributions.

The origin of the decreased activity and increased methane selectivity of small Co NPs was investigated by de Jong's group using steady-state isotopic transient kinetic analysis (SSITKA) to monitor the surface species[38]. The irreversibly bonded CO molecules should be responsible for the low activity of small NPs due to the block of Co sites. Besides, the lower specific activity of terrace sites on smaller Co particles seems to significantly hamper the TOF. The possible explanation could be the slower CH_x hydrogenation caused by the stronger binding of Co-CH_x bond. Salmeron's group demonstrates the decreased CO conversion to methane with particle size (< 10 nm) is not due to surface oxidation by water, carbon deposition or sintering[44]. Instead,

they proved that H_2 dissociation is more difficult on smaller particles via H-D exchange experiments, and proposed the observed size effect is related to the dissociation of hydrogen.

3.2 Effect of surface oxidation state

Besides size effect, the investigation into other characteristics of catalysts will bring more insights into the reaction mechanism and catalyst design, among which the oxidation states of surface metals catches our attention. It is well known from surface chemistry that surface restructuring can be induced by various gases, which could lead to the activation of the catalyst surface or new reaction pathways[52-54].In F-T synthesis, metallic Co is believed to be necessary to dissociate CO, which most likely works as the active site. Nevertheless, the oxidation of surface cobalt atoms is inevitable in the reaction pathway, as shown in equation 4.

$$CO + H_2 + Co \rightarrow CH_2 + CoO \quad (4)$$

$$CoO + H_2 \rightarrow H_2O + Co \quad (5)$$

The surface oxygen could be subsequently removed by reacting with hydrogen, producing water and regenerating the cobalt active sites (equation 5). The byproduct water, however, is also an oxidizing agent, that possibly leads to the deactivation of cobalt catalysts due to surface oxidation. The impact of water in F-T synthesis has been well summarized in the previous reviews[55-58]. Theoretically, the regeneration of metallic Co active sites of bulk cobalt oxides is thermodynamically favorable at the typical operation temperature for F-T synthesis (220-250 ˚C). On the other hand, small Co NPs (< 4.4 nm, unsupported) are expected to be unstable in the presence of water vapor (pH_2O/pH_2 < 1.5, ~ 75% CO conversion) and oxidized to Co(II)O, as evidenced by the thermodynamic analysis[59]. The ease of oxidation of smaller Co NPs might decrease the number of active sites and thus lead to poor activity, which is another explanation of size effect on the activity. Khodakov's group provided direct evidence for surface oxidation of Al_2O_3 supported Co NPs using scanning transmission electron microscopy combined with spatially resolved electron energy loss spectroscopy (STEM-EELS)[60]. The tested Co NPs stay almost metallic (both in the bulk and at the surface) after 20 h reaction at 220 ˚C. Cobalt oxide species showed up after severer reaction conditions and longer reaction time (240 ˚C, 170 h) were applied. When temperature increases to 340 ˚C, a distinct oxygen halo was appeared in STEM, indicating

the formation of CoO_x layer on metallic Co core, in the presence of dominant water vapor at higher temperatures. A decreased activity and increased selectivity to methane were observed for this surface-oxidized Co NPs.

It is noteworthy that oxidized cobalt atoms rather than metallic cobalt could interact with the support, yielding the thermodynamically more stable species (e.g. cobalt aluminate[61], cobalt silicate[62] or cobalt titanate[63]), which further deactivates the catalysts due to the loss of active cobalt. Holmen's group investigates Co reoxidation via in situ X-ray absorption near edge structure (XANES) and confirmed the accumulation of $CoAl_2O_4$ during the F-T process[64]. They proposed the spreading of formed CoO over the Al_2O_3 leads to the reaction of Co^{2+} with the support. To avoid the irreversible loss of active species, the authors suggest a reoxidation threshold calculated as 5.3 nm. Besides making larger particles, the stability of metallic phases could also be increased by the addition of promoters such as Pt[65], Re[66, 67] and Ru[45]. For example, Pt could promote the reduction of calcined Co catalysts for both steps at relatively lower temperatures: $Co_3O_4 \rightarrow$ CoO and CoO $\rightarrow Co^0$[68]. With the lower activation energy of forming cobalt metallic phase, the reaction rate was significantly increased compared to monometallic Co NPs.

Interestingly, our group discovered an active cobalt oxide catalyst for the F-T Synthesis[25]. Two porous metal oxides (i.e. TiO_2 and SiO_2) were prepared to support 10 nm Co NPs synthesized by colloidal method. For both supports, a reduced Co (denoted as "red") catalyst and an oxidized Co (denoted as "ox") catalyst were prepared. The reduced Co was pretreated in 20 vol% H_2 in He flow at 450 ˚C for 1h. The oxidized Co was obtained by pure O_2 treatment at 350 ˚C, followed by H_2 treatment at 250 ˚C which is not sufficient to reduce cobalt. Ambient-Pressure X-ray Photoelectron Spectroscopy (AP-XPS) spectra of Co/TiO_2 demonstrates that Ti species were all reduced to Ti^{3+} at 450 ˚C under 100 mTorr of H_2 while Co^{n+} was only partially reduced to metallic Co^0 (Fig. 2a-b). As a comparison, no metallic Co was observed at 250 ˚C and Ti was only partially reduced. The oxidation state of Co was further analyzed by Extended X-ray Absorption Fine Structure (EXAFS), showing the metallic Co at 450 ˚C and oxidized Co at 250 ˚C under 150 Torr H_2 (Fig.2c-d), which pressure is closer to the reaction conditions. F-T synthesis at 250 ˚C under 5 atm CO/H_2

(ratio 1:2) for 24 h was then catalyzed by both Co/TiO_2 and Co/SiO_2 with alternating oxidation states. Co/TiO_2 shows a larger TOF than that of Co/SiO_2 all over the time. Surprisingly, the oxidized Co/TiO_2 is active and yields 2 times TOF compared to reduced Co/TiO_2. In contrast, reduced Co/SiO_2 is more active compared to oxidized Co/SiO_2. To understand the unusual catalytic performance, the surface Co percentage (%Co) on TiO_2 support was monitored by both AP-XPS and lab-based XPS. It was found out the %Co increased from 29% in O_2 at 350 ˚C to 35% in H_2 at 250 ˚C, but dropped to 20% at 450 ˚C in H_2. The decreased surface %Co in the reduced Co/TiO_2 was probably due to the encapsulation of metallic Co by TiO_2 (Fig.2e), which lowers the number of accessible active sites and thus hamper the activity. Meanwhile, the increase of %Co in the oxidized Co/TiO_2 indicates the wetting of small cobalt oxide on the surface of TiO_2 due to the strong metal-support interaction (SMSI).

A recent work by Liu and coworkers also observed an active CoO phase supported by SiO_2 in F-T synthesis[69]. Differently, the CoO species were obtained directly from the reduction of Co_3O_4 and yielded higher TOF compared to metallic Co. The DFT calculation demonstrated the lower activation energy of CO dissociation via hydrogen-assisted CH_2O pathway on CoO(200) surface compared to the face-center cubic Co (111) surface, suggesting CoO could also be an active phase in this reaction.

3.3 Effect of crystal phase

Crystallographic structure is another structure sensitivity observed in F-T synthesis. Cobalt can exist in three different crystal phases, i.e., α-Co (HCP, hexagonal closest packed), β-Co (FCC, face-centered cubic) and ε-Co (complex cP structure, primitive cubic)[70]. While the β-α phase transition of bulk Co occurs around 400 ˚C[71], the transformation of NPs could be achieved at milder condition. Kitakami discovered a close relationship between the crystal phase and particle size, namely pure FCC (<20 nm), mixture of FCC and HCP (~ 30 nm) and dominant HCP with a very small portion of FCC (> 40 nm). A further theoretical calculation suggested β-Co Wulff polyhedron is the most stable phase when particles are smaller than 110 nm, while the other two (β-MT icosahedron, α- Wulff polyhedron) could exist as metastable phases[72]. The difference in crystal structure leads to distinct surface morphologies and topologies (i.e. exposed facets, atom density, active sites), which results in different catalytic performance. Many groups have reported

the higher activity of HCP than FCC Co NPs[73-78]. A detailed DFT calculation reveals the higher CO dissociation rate on most of the HCP facets compared to those of FCC, indicating the higher intrinsic activity of HCP Co[79]. Moreover, the computational results suggest the direct CO dissociation ($CO^* + H^* \rightarrow C^* + O^* + H^*$) is preferred on HCP Co while the hydrogen-assisted CO dissociation ($CO^* + H^* \rightarrow CHO^* \rightarrow CH^* + O^*$) is thermodynamically favored on FCC Co NP. As shown in Fig.3, the potential energy of direct pathway on HCP Co is lower than that of hydrogen-assisted dissociation on FCC Co, indicating the higher activity of HCP Co even in the presence of H_2.

The formation of Co_2C during F-T synthesis was also observed, which is considered as one of the deactivation mechanisms[23, 80]. Co_2C is typically regarded inactive, yielding very low activity of CO dissociation and high selectivity to methane[78, 81]. However, Co_2C nanoprisms derived from $Co_xMn_{1-x}O$ under reaction conditions were reported to selectively convert CO to low olefins[82]. It is believed the exposed {101} and {020} facets in the quadrangular nanoprism morphology are responsible for activity and high selectivity to lower olefins. In another work by Li's group[83], the selectivity towards alcohols dramatically increases in the presence of both Co_2C and metallic cobalt, and therefore the Co_2C and Co interface was proposed as the active sites. DFT was used to confirm the synergetic effect of Co-Co_2C. The calculation results suggest dissociative adsorption of CO and subsequent C-C coupling occur on the metallic Co sites, while Co_2C preferred the non-dissociative adsorption of CO molecules which could easily insert into the CH_2 intermediates on the Co sites to produce alcohol. Another recent computational work investigates the Co, Co_2C and Co_3C phases to determine the intrinsic active site for selective formation of light olefin in FTS[84]. The calculation indicates the formation of alkanes is thermodynamically favored on Co(111), while Co_2C(111) has the highest selectivity to methane due to the stronger binding of CH_2 intermediates. Furthermore, Co_3C(101) is beneficial to increase the selectivity of light olefins due to its lower energy barrier for C-C coupling and weaker H binding suppressing the deep hydrogenation. Finally, the authors suggest the Co/Co_3C interface could be a promising candidate for the selective production of light olefins, as summarized in Fig.4.

3.4 Bimetallic nanoparticles

As has been discussed, Co-based catalysts produce hydrocarbons with high carbon numbers but few oxygenated products which require a different reaction pathway. Nanoparticles composed of two different metal elements usually show novel catalytic, electronic and optical properties compared to the two individual metals[85-87]. The modification of the activity and selectivity of catalytic reactions results from the tunable electronic and geometric properties by adding the second metal[54, 88].

Rhodium was selected due to its ability to absorb CO molecules both dissociatively and non-dissociatively[89], the latter is believed to be critical in alcohol formation[90]. We thus were able to adjust the alcohol selectivity by tuning the amount of added rhodium. 5 nm spherical Co-Rh bimetallic NPs (with 2, 10, 16 at% Rh), pure Co and Rh NPs were synthesized by the colloidal method[26]. These nanoparticles were then supported on MCF-17 and used as catalysts in F-T synthesis. Co-Rh bimetallic catalysts show a similar activity compared to the pure Co catalysts, while pure Rh remains almost inactive. The addition of Rh changes the selectivity compared to pure Co catalyst. Although the high selectivity towards C_{5+} is similar to that of Co/MCF-17, alcohols including methanol, ethanol and propanol were produced by Co-Rh/MCF-17, with up to 5 times higher yields. In order to build the relationship between the catalytic properties and surface structures, Co and Rh distribution under reaction conditions were investigated by AP-XPS. Fig. 5a shows the phase segregation induced by different gas environments. Surface Co is enriched to 88% after O_2 treatment at 350 ˚C, while Rh diffused to the surface under H_2 flow at 450 ˚C, and remained on the surface (59%) under reaction gas environment (H_2: CO = 2:1). Probing depth profiles of AP-XPS indicates the decrease of Rh concentration from the surface to the bulk, confirming the surface enrichment of Rh (Fig.5b). The alcohol selectivity is then correlated to the surface Rh concentration. A volcano shape was observed for both alcohol formation (Fig 5c) and selectivity to larger alcohols such as propanol (Fig. 5d), clearly indicating an optimum Co-Rh ratio on the surface is critical to enhancing the selectivity.

4 Chemical Transient Kinetics study

F-T synthesis is a complicated reaction involving plenty of elementary steps, reaction active sites and surface spices, of which reaction mechanism is still under debate. Transient kinetics studies are very useful to gain fundamental insights into intrinsic reaction kinetics and reaction mechanism. Transient techniques such as steady-state isotope kinetics analysis (SSITKA)[91, 92], temporal analysis of products (TAP)[93], and chemical transient kinetics (CTK)[94] have been applied in the heterogeneous catalysis for mechanistic and kinetic investigation. Here, the design of CTK system in our group and its application in the mechanism study of F-T synthesis will be reviewed and discussed in this section.

4.1 System set-up

CTK monitors the time response of the F-T synthesis following a sudden change from inert gases to reactants (CO and H_2) and traces the build-up of the steady state. Insights are gained into the initial construction of the active surface, thus to help understand the full scope of each step and better control the selectivity of this complicated reaction. A new gas flow system with two independent plug-flow circuits was designed for CTK experiments[28]. As shown in Fig.6 inset, a four-way valve is used to control the circuit directed through the reactor. The gas at the reactor outlet was continuously analyzed by an online quadrupole mass spectrometer (QMS), which operates using a multiple ion detection mode with an effective time resolution of 2.2s. To obtain a complete picture of the broad product distribution, samples at the outlet were also analyzed offline using a GC-MS equipped with a flame ionization detector (FID), a thermal conductivity detector (TCD) and a QMS. A model catalyst CoMgO was used to evaluate the performance of the system, and the results from online-QMS are consistent with the previous report, confirming the validity of the system. Followed by that, GC-MS was used as the analyzer for CTK experiments. A small volume of the effluent gas (~1.3 mL, corresponding to the time resolution of 2 s) is injected into a vacuum-sealed flask via a synchronized sampling system at moments during the transient period (the selected sampling times were marked as the vertical dashed line in Fig.7a). These samples were then analyzed by GC-MS to provide a product distribution at each time (t), and the selectivity of different products as a function of time was displayed in Fig.7b. The main product methane is the first one to appear, followed by C_{2s}, C_{3s}, C_{4s}, C_{5s} and C_{6s}, all appearing in the first 40 s. The product distribution reached the steady state after 60 s and remained unchanged over a few hours.

The appearance sequence of hydrocarbons is directly related to the carbon numbers, indicating a polymerization mechanism. The use of GC greatly lowers the detecting limit compared to only using online QMS where C_{4+} is not detectable.

4.2 Time-Resolved CTK study of model Co catalysts.

The reaction mechanism of FTS is still under debate. As summarized in previous reviews[95-99], three main mechanisms were proposed, namely carbide mechanism, hydroxycarbene (enol) mechanism and CO insertion mechanism. Fischer and Thopsch proposed the carbide mechanism[100], suggesting the dissociative adsorption of CO as chain initiation. Methylene (CH_2) group formed by hydrogenation of surface carbon is believed to be the monomer of chain propagation. Hydroxycarbene (-CHOH) intermediates are responsible for C-C coupling in hydroxycarbene mechanism[101], while inserting CO into alkyl intermediates represents the chain growth in CO insertion mechanism[102], as summarized in Fig.8. Due to the complicated reaction network, multiple active sites or ensembles are likely involved in F-T synthesis for individual steps: CO dissociation, H_2 dissociation, monomer formation, polymerization, chain termination. To better understand the reaction mechanism and reveal the structure-property relationship, transient reactor systems such as CTK and SSITKA have been applied to provide information about surface coverage and residence time of intermediates[92, 94, 95, 103-105]. For example, SSITKA was used to determine the rate coefficient of chain initiation, growth and termination in F-T synthesis[106] and a previous CTK study showed the evidence of CO-insertion mechanism on Co/MgO model catalyst[104]. Besides, Hensen's group used both SSITKA and CTK to investigate the mechanism of methanation over Pt-prompted Co/SiO_2 catalysts[107].

Somorjai and coworkers presents a CTK study on the size dependence of Co NPs (4.3 nm and 9.5 nm) under non-steady states condition[27]. Similar to the CoMgO catalyst discussed in section 4.1, hydrocarbons appeared in the order of the carbon numbers (Fig.7a-b). This consistent sequential appearance of the hydrocarbons confirms that single carbon species are the monomer on both Co NPs, agreeing with the Anderson-Schulz-Flory distribution. The single carbon monomer is further proved during backward transient that a significant amount of methane was detected in 10 s after CO purge is stopped. The carbon balance was traced over time using data from both online MS and offline GC-MS, and carbon coverage (Θ_c) as a function of time was plotted for both catalysts (Fig. 9d). Both catalysts have a change of accumulating rate around 15 s, with 4.3 nm Co NPs tend

to be stabilized at $\theta_c = 0.5$ while 9.5 nm Co NPs continue to steadily grow carbon on the surface. Therefore, we propose the carbon monomer is formed in the first several seconds. Besides, θ_c the value of 0.5 might also be critical where carbon coverage and hydrogen coverage reache equilibrium and favors the chain-growth kinetics. The product distribution of both Co NPs was obtained from GC-MS. A small amount of CO_2 was observed on both catalysts, but no alcohol was detected for either of them. The only big difference is the olefin to paraffin ratios (O/P). The smaller O/P value of 4.3 nm Co (0.07 vs. 0.35) indicates the higher hydrogenation activity of smaller Co NPs. Fig. 9c shows the different normalized outlet flow of CO for both catalysts monitored by online QMS. 4.3 nm Co has a shaper slope and reaches the steady-state in 20 s, indicating a faster adjustment of the surface under the reaction environment even its surface area is larger. As a contrast, it takes about 100 s for 9.5 nm Co NPs to reach the steady state, probably owing to the weak adsorption of CO.

A recent CTK study by Kruse's group revealed the competing mechanisms in F-T synthesis over Co-MnO_x model catalysts[108]. CO insertion mechanism is believed to be dominant under high surface coverage condition, evidenced by the linear dependence of transient chain lengthening probability on the CO partial pressure. However, the C-C coupling of CH_x is also significant below the monolayer limit, probably via the hydrogen-assisted CO dissociation. This study demonstrated the importance of surface coverage on the reaction pathways and highlighted the advantages of CTK systems in monitoring the surface intermediates.

5 Summary and outlook

We showed a general methodology to study the Co-based catalysts for F-T synthesis, including the enhancement of catalytic performance via particle size effect, surface oxidation state, support effect and alloying to form bimetallic nanoparticles. All these parameters played critical roles in tuning the reaction activity and selectivity, making F-T synthesis a very complicated reaction network. The Co size effect has been studied for many years, and many understandings of the origin of Co size effect were achieved. Clearly, the size effect also correlates with the effect of surface oxidation state and particle crystal phases, and thus a comprehensive study to integrate these elements might be helpful. The oxides and carbides which were previously believed to be responsible for deactivation, have been reported as active phases with different selectivity from metallic cobalt. The design of novel cobalt oxide and cobalt carbide could lead to production

distribution shift to lower olefins or alcohols, leading to a new reaction direction. Moreover, CTK has been proven to be a powerful tool to investigate the reaction kinetics and mechanism during the non-steady state, but mostly on model catalysts. More catalytic systems should be investigated using transient techniques to build a complete picture of F-T synthesis. For our group, it is planned to continue study F-T synthesis using single site catalyst with different metal atoms and metal oxide supports. We envision novel catalytic behaviors will be observed on single site catalyst due to its unique adsorption geometry, tunable oxidation state via SMSI and good thermal stability.

Conflict of interest

The authors declare that they have no known competing financial interests or personal relationships that could have appeared to influence the work reported in this paper.

Acknowledgments

The work shown in this paper was supported by support from the Director, Office of Basic Energy Sciences, Division of Chemical Sciences, Geological and Biosciences of the U.S. Department of Energy under contract no. DE-AC02-05CH11231.

CRediT authorship contribution statement

Zhiyuan Qi: Conceptualization, writing- Original draft preparation, review& editing
Luning Chen: Writing- reviewing and editing
Shuchen Zhang: visualization
Ji Su: Conceptualization
Gabor A. Somorjai: Supervision, Conceptualization

References

[1] J.R. Rostrup-Nielsen, Catal Today, 63 (2000) 159-164.

[2] N. Abatzoglou, C. Fauteux-Lefebvre, Wires Energy Environ, 5 (2016) 169-187.

[3] K.Z. Li, R. Zhang, J.C. Bi, Int J Hydrogen Energ, 35 (2010) 2722-2726.

[4] M.M. Yung, W.S. Jablonski, K.A. Magrini-Bair, Energ Fuel, 23 (2009) 1874-1887.

[5] I. WENDER, Annual review of energy, 11 (1986) 295-314.

[6] A. Hussain, S.R. Guiot, P. Mehta, V. Raghavan, B. Tartakovsky, Appl Microbiol Biot, 90 (2011) 827-836.
[7] D. Andriamasinoro, R. Kieffer, A. Kiennemann, P. Poix, Appl Catal A-Gen, 106 (1993) 201-212.
[8] F.A.P. Cavalcanti, A.Y. Stakheev, W.M.H. Sachtler, J Catal, 134 (1992) 226-241.
[9] J.B. Wang, Q. Sun, S. Chan, H.B. Su, Appl Catal A-Gen, 509 (2016) 97-104.
[10] M. Chaos, F.L. Dryer, Combust Sci Technol, 180 (2008) 1053-1096.
[11] H. Gruber, P. Groß, R. Rauch, A. Reichhold, R. Zweiler, C. Aichernig, S. Müller, N. Ataimisch, H. Hofbauer, Biomass Conversion and Biorefinery, (2019).
[12] H. Schulz, Appl Catal A-Gen, 186 (1999) 3-12.
[13] S. Mousavi, A. Zamaniyan, M. Irani, M. Rashidzadeh, Appl Catal A-Gen, 506 (2015) 57-66.
[14] B.C. Enger, A. Holmen, Catal Rev, 54 (2012) 437-488.
[15] L. Bruce, J.F. Mathews, Appl Catal, 4 (1982) 353-369.
[16] H.M.T. Galvis, K.P. de Jong, ACS Catal, 3 (2013) 2130-2149.
[17] S. Abello, D. Montane, Chemsuschem, 4 (2011) 1538-1556.
[18] D.B. Bukur, B. Todic, N. Elbashir, Catal Today, 275 (2016) 66-75.
[19] N.S. Govender, M.J. van Vuuren, M. Claeys, E. van Steen, Ind Eng Chem Res, 45 (2006) 8629-8633.
[20] E. de Smit, B.M. Weckhuysen, Chem Soc Rev, 37 (2008) 2758-2781.
[21] A.Y. Khodakov, W. Chu, P. Fongarland, Chem Rev, 107 (2007) 1692-1744.
[22] E. Rytter, A. Holmen, Catalysts, 5 (2015) 478-499.
[23] N.E. Tsakoumis, M. Ronning, O. Borg, E. Rytter, A. Holmen, Catal Today, 154 (2010) 162-182.
[24] G. Melaet, A.E. Lindeman, G.A. Somorjai, Top Catal, 57 (2014) 500-507.
[25] G. Melaet, W.T. Ralston, C.S. Li, S. Alayoglu, K. An, N. Musselwhite, B. Kalkan, G.A. Somorjai, J Am Chem Soc, 136 (2014) 2260-2263.
[26] W.C. Liu, G. Melaet, W.T. Ralston, S. Alayoglu, Y. Horowitz, R. Ye, T. Hurlburt, B.H. Mao, E. Crumlin, M. Salmeron, G.A. Somorjai, Catal Lett, 146 (2016) 1574-1580.
[27] W.T. Ralston, G. Melaet, T. Saephan, G.A. Somorjai, Angew Chem Int Edit, 56 (2017) 7415-7419.
[28] G. Melaet, W.T. Ralston, W.C. Liu, G.A. Somorjai, J Phys Chem C, 118 (2014) 26921-26925.

[29] R.J. Moon, A. Martini, J. Nairn, J. Simonsen, J. Youngblood, Chem Soc Rev, 40 (2011) 3941-3994.
[30] K. An, Q. Zhang, S. Alayoglu, N. Musselwhite, J.Y. Shin, G.A. Somorjai, Nano Lett, 14 (2014) 4907-4912.
[31] K.M. Bratlie, H. Lee, K. Komvopoulos, P.D. Yang, G.A. Somorjai, Nano Lett, 7 (2007) 3097-3101.
[32] L.N. Chen, K.P. Hou, Y.S. Liu, Z.Y. Qi, Q. Zheng, Y.H. Lu, J.Y. Chen, J.L. Chen, C.W. Pao, S.B. Wang, Y.B. Li, S.H. Xie, F.D. Liu, D. Prendergast, L.E. Klebanoff, V. Stavila, M.D. Allendorf, J.H. Guo, L.S. Zheng, J. Su, G.A. Somorjai, J Am Chem Soc, 141 (2019) 17995-17999.
[33] S.H. Joo, J.Y. Park, J.R. Renzas, D.R. Butcher, W.Y. Huang, G.A. Somorjai, Nano Lett, 10 (2010) 2709-2713.
[34] C.J. Kliewer, C. Aliaga, M. Bieri, W.Y. Huang, C.K. Tsung, J.B. Wood, K. Komvopoulos, G.A. Somorjai, J Am Chem Soc, 132 (2010) 13088-13095.
[35] H. Song, R.M. Rioux, J.D. Hoefelmeyer, R. Komor, K. Niesz, M. Grass, P.D. Yang, G.A. Somorjai, J Am Chem Soc, 128 (2006) 3027-3037.
[36] H.L. Wang, A. Sapi, C.M. Thompson, F.D. Liu, D. Zherebetskyy, J.M. Krier, L.M. Carl, X.J. Cai, L.W. Wang, G.A. Somorjai, J Am Chem Soc, 136 (2014) 10515-10520.
[37] G.L. Bezemer, J.H. Bitter, H.P.C.E. Kuipers, H. Oosterbeek, J.E. Holewijn, X.D. Xu, F. Kapteijn, A.J. van Dillen, K.P. de Jong, J Am Chem Soc, 128 (2006) 3956-3964.
[38] J.P. den Breejen, P.B. Radstake, G.L. Bezemer, J.H. Bitter, V. Froseth, A. Holmen, K.P. de Jong, J Am Chem Soc, 131 (2009) 7197-7203.
[39] H.M.T. Galvis, J.H. Bitter, T. Davidian, M. Ruitenbeek, A.I. Dugulan, K.P. de Jong, J Am Chem Soc, 134 (2012) 16207-16215.
[40] T. Herranz, X.Y. Deng, A. Cabot, J.G. Guo, M. Salmeron, J Phys Chem B, 113 (2009) 10721-10727.
[41] G. Prieto, A. Martinez, P. Concepcion, R. Moreno-Tost, J Catal, 266 (2009) 129-144.
[42] S. Rane, O. Borg, E. Rytter, A. Holmen, Appl Catal A-Gen, 437 (2012) 10-17.
[43] O. Borg, P.D.C. Dietzel, A.I. Spjelkavik, E.Z. Tveten, J.C. Walmsley, S. Diplas, S. Eri, A. Holmen, E. Ryttera, J Catal, 259 (2008) 161-164.

[44] A. Tuxen, S. Carenco, M. Chintapalli, C.H. Chuang, C. Escudero, E. Pach, P. Jiang, F. Borondics, B. Beberwyck, A.P. Alivisatos, G. Thornton, W.F. Pong, J.H. Guo, R. Perez, F. Besenbacher, M. Salmeron, J Am Chem Soc, 135 (2013) 2273-2278.
[45] E. Iglesia, Appl Catal A-Gen, 161 (1997) 59-78.
[46] A. Martinez, C. Lopez, F. Marquez, I. Diaz, J Catal, 220 (2003) 486-499.
[47] G.L. Bezemer, A. van Laak, A.J. van Dillen, K.P. de Jong, Stud Surf Sci Catal, 147 (2004) 259-264.
[48] S.L. Soled, E. Iglesia, R.A. Fiato, J.E. Baumgartner, H. Vroman, S. Miseo, Top Catal, 26 (2003) 101-109.
[49] J.L. Zhang, J.A. Chen, J. Ren, Y.W. Li, Y.H. Sun, Fuel, 82 (2003) 581-586.
[50] E. Iglesia, S.L. Soled, R.A. Fiato, J Catal, 137 (1992) 212-224.
[51] N. Fischer, E. van Steen, M. Claeys, J Catal, 299 (2013) 67-80.
[52] B. Eren, D. Zherebetskyy, L.L. Patera, C.H. Wu, H. Bluhm, C. Africh, L.W. Wang, G.A. Somorjai, M. Salmeron, Science, 351 (2016) 475-478.
[53] F. Tao, S. Dag, L.W. Wang, Z. Liu, D.R. Butcher, H. Bluhm, M. Salmeron, G.A. Somorjai, Science, 327 (2010) 850-853.
[54] F. Tao, M.E. Grass, Y.W. Zhang, D.R. Butcher, J.R. Renzas, Z. Liu, J.Y. Chung, B.S. Mun, M. Salmeron, G.A. Somorjai, Science, 322 (2008) 932-934.
[55] A.K. Dalai, B.H. Davis, Appl Catal A-Gen, 348 (2008) 1-15.
[56] E. Rytter, A. Holmen, ACS Catal, 7 (2017) 5321-5328.
[57] V.R.R. Pendyala, G. Jacobs, J.C. Mohandas, M.S. Luo, H.H. Hamdeh, Y.Y. Ji, M.C. Ribeiro, B.H. Davis, Catal Lett, 140 (2010) 98-105.
[58] M. Claeys, E. van Steen, Catal Today, 71 (2002) 419-427.
[59] E. van Steen, M. Claeys, M.E. Dry, J. van de Loosdrecht, E.L. Viljoen, J.L. Visagie, J Phys Chem B, 109 (2005) 3575-3577.
[60] C. Lancelot, V.V. Ordomsky, O. Stephan, M. Sadeqzadeh, H. Karaca, M. Lacroix, D. Curulla-Ferre, F. Luck, P. Fongarland, A. Griboval-Constant, A.Y. Khodakov, ACS Catal, 4 (2014) 4510-4515.
[61] G. Jacobs, P.M. Patterson, T.K. Das, M.S. Luo, B.H. Davis, Appl Catal A-Gen, 270 (2004) 65-76.
[62] J.G. Chen, H.W. Xiang, H.Y. Gao, Y.H. Sun, React Kinet Catal L, 73 (2001) 169-177.

[63] K. Jalama, N.J. Coville, D. Hildebrandt, D. Glasser, L.L. Jewell, J.A. Anderson, S. Taylor, D. Enache, G.J. Hutchings, Top Catal, 44 (2007) 129-136.
[64] N.E. Tsakoumis, J.C. Walmsley, M. Ronning, W. van Beek, E. Rytter, A. Hohnen, J Am Chem Soc, 139 (2017) 3706-3715.
[65] J.L. Li, X.D. Zhan, Y.Q. Zhang, G. Jacobs, T. Das, B.H. Davis, Appl Catal A-Gen, 228 (2002) 203-212.
[66] M. Rothaemel, K.F. Hanssen, E.A. Blekkan, D. Schanke, A. Holmen, Catal Today, 38 (1997) 79-84.
[67] G. Jacobs, J.A. Chaney, P.M. Patterson, T.K. Das, B.H. Davis, Appl Catal A-Gen, 264 (2004) 203-212.
[68] W. Chu, P.A. Chernavskii, L. Gengembre, G.A. Pankina, P. Fongarland, A.Y. Khodakov, J Catal, 252 (2007) 215-230.
[69] X.J. Fang, B. Liu, K. Cao, P.J. Yang, Q. Zhao, F. Jiang, Y.B. Xu, R. Chen, X.H. Liu, ACS Catal, 10 (2020) 2799-2816.
[70] C.S. Yoo, P. Soderlind, H. Cynn, J Phys-Condens Mat, 10 (1998) L311-L318.
[71] M. Hansen, R.P. Elliott, F.A. Shunk, Constitution of binary alloys, McGraw-Hill, New York, 1958.
[72] O. Kitakami, H. Sato, Y. Shimada, F. Sato, M. Tanaka, Phys Rev B, 56 (1997) 13849-13854.
[73] O. Ducreux, B. Rebours, J. Lynch, M. Roy-Auberger, D. Bazin, Oil Gas Sci Technol, 64 (2009) 49-62.
[74] D.I. Enache, B. Rebours, M. Roy-Auberger, R. Revel, J Catal, 205 (2002) 346-353.
[75] M.K. Gnanamani, G. Jacobs, W.D. Shafer, B.H. Davis, Catal Today, 215 (2013) 13-17.
[76] H. Karaca, O.V. Safonova, S. Chambrey, P. Fongarland, P. Roussel, A. Griboval-Constant, M. Lacroix, A.Y. Khodakov, J Catal, 277 (2011) 14-26.
[77] V.A.D.P. O'Shea, N. Homs, J.L.G. Fierro, P.R. de la Piscina, Catal Today, 114 (2006) 422-427.
[78] M. Sadeqzadeh, H. Karaca, O.V. Safonova, P. Fongarland, S. Chambrey, P. Roussel, A. Griboval-Constant, M. Lacroix, D. Curulla-Ferre, F. Luck, A.Y. Khodakov, Catal Today, 164 (2011) 62-67.
[79] J.X. Liu, H.Y. Su, D.P. Sun, B.Y. Zhang, W.X. Li, J Am Chem Soc, 135 (2013) 16284-16287.
[80] P.K. Agrawal, J.R. Katzer, W.H. Manogue, J Catal, 69 (1981) 312-326.

[81] A.V. Puga, Catal Sci Technol, 8 (2018) 5681-5707.
[82] L.S. Zhong, F. Yu, Y.L. An, Y.H. Zhao, Y.H. Sun, Z.J. Li, T.J. Lin, Y.J. Lin, X.Z. Qi, Y.Y. Dai, L. Gu, J.S. Hu, S.F. Jin, Q. Shen, H. Wang, Nature, 538 (2016) 84-+.
[83] Y.P. Pei, J.X. Liu, Y.H. Zhao, Y.J. Ding, T. Liu, W.D. Dong, H.J. Zhu, H.Y. Su, L. Yan, J.L. Li, W.X. Li, ACS Catal, 5 (2015) 3620-3624.
[84] B. Liu, W.P. Li, Y.B. Xu, Q. Lin, F. Jiang, X.H. Liu, ACS Catal, 9 (2019) 7073-7089.
[85] Z.Y. Qi, C.X. Xiao, C. Liu, T.W. Goh, L. Zhou, R. Maligal-Ganesh, Y.C. Pei, X.L. Li, L.A. Curtiss, W.Y. Huang, J Am Chem Soc, 139 (2017) 4762-4768.
[86] Y.C. Pei, Z.Y. Qi, T.W. Goh, L.L. Wang, R.V. Maligal-Ganesh, H.L. MacMurdo, S.R. Zhang, C.X. Xiao, X.L. Li, F. Tao, D.D. Johnson, W.Y. Huang, J Catal, 356 (2017) 307-314.
[87] R.V. Maligal-Ganesh, C.X. Xiao, T.W. Goh, L.L. Wang, J. Gustafson, Y.C. Pei, Z.Y. Qi, D.D. Johnson, S.R. Zhang, F. Tao, W.Y. Huang, ACS Catal, 6 (2016) 1754-1763.
[88] F. Tao, M.E. Grass, Y.W. Zhang, D.R. Butcher, F. Aksoy, S. Aloni, V. Altoe, S. Alayoglu, J.R. Renzas, C.K. Tsung, Z.W. Zhu, Z. Liu, M. Salmeron, G.A. Somorjai, J Am Chem Soc, 132 (2010) 8697-8703.
[89] R. Burch, M.I. Petch, Appl Catal A-Gen, 88 (1992) 39-60.
[90] X.L. Pan, Z.L. Fan, W. Chen, Y.J. Ding, H.Y. Luo, X.H. Bao, Nat Mater, 6 (2007) 507-511.
[91] S.L. Shannon, J.G. Goodwin, Chem Rev, 95 (1995) 677-695.
[92] C. Ledesma, J. Yang, D. Chen, A. Holmen, ACS Catal, 4 (2014) 4527-4547.
[93] J. Perez-Ramirez, E.V. Kondratenko, Catal Today, 121 (2007) 160-169.
[94] A. Frennet, T.V. de Bocarme, J.M. Bastin, N. Kruse, J Phys Chem B, 109 (2005) 2350-2359.
[95] Y.Y. Qi, J. Yang, D. Chen, A. Holmen, Catal Lett, 145 (2015) 145-161.
[96] J. Cheng, P. Hu, P. Ellis, S. French, G. Kelly, C.M. Lok, Top Catal, 53 (2010) 326-337.
[97] M.C. Valero, P. Raybaud, Catal Lett, 143 (2013) 1-17.
[98] R.A. van Santen, A.J. Markvoort, I.A.W. Filot, M.M. Ghouri, E.J.M. Hensen, Phys Chem Chem Phys, 15 (2013) 17038-17063.
[99] E. van Steen, M. Claeys, Chem Eng Technol, 31 (2008) 655-666.
[100] F. Fischer, H. Tropsch, Ber Dtsch Chem Ges, 59 (1926) 830-831.
[101] J.T. Kummer, P.H. Emmett, J Am Chem Soc, 75 (1953) 5177-5183.
[102] H. Pichler, H. Schulz, Chem-Ing-Tech, 42 (1970) 1162-&.
[103] G. Melaet, W.T. Ralston, W.C. Liu, G.A. Somorjai, Catal Today, 272 (2016) 69-73.

[104] J. Schweicher, A. Bundhoo, N. Kruse, J Am Chem Soc, 134 (2012) 16135-16138.
[105] R.J. Berger, F. Kapteijn, J.A. Moulijn, G.B. Marin, J. De Wilde, M. Olea, D. Chen, A. Holmen, L. Lietti, E. Tronconi, Y. Schuurman, Appl Catal A-Gen, 342 (2008) 3-28.
[106] K.R. Krishna, A.T. Bell, J Catal, 139 (1993) 104-118.
[107] W. Chen, R. Pestman, B. Zijlstra, I.A.W. Filot, E.J.M. Hensen, ACS Catal, 7 (2017) 8050-8060.
[108] M. Athariboroujeny, A. Raub, V. Iablokov, S. Chenakin, L. Kovarik, N. Kruse, ACS Catal, 9 (2019) 5603-5612.

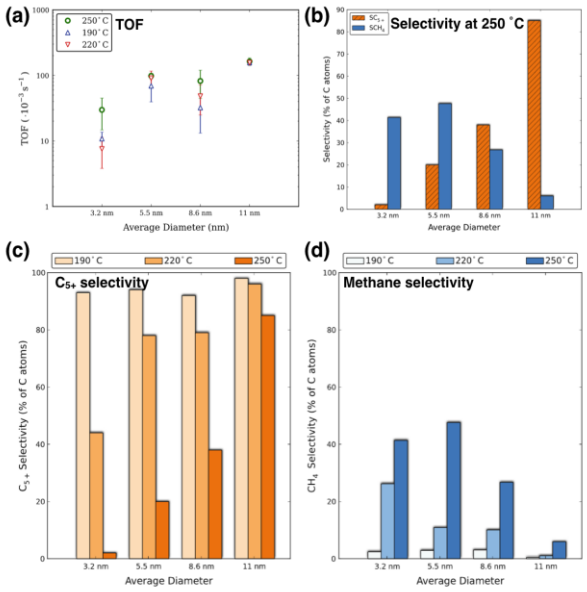

Fig.1 (a) CO consumption TOF of 3.2, 5.5, 8.6 and 11 nm Co/MCF-17 catalysts at three temperatures (190, 220, 250 ˚C). CO hydrogenation was carried out at 4 bar with H_2 to CO ratio of 2:1; (b) Selectivity towards methane (SCH_4) and hydrocarbons with the carbon number of 5 and higher (SC_{5+}) as a function of particle size in CO hydrogenation at 5 bar and 250 ˚C. Temperature and size dependent of (c) C_{5+} and (d) methane selectivity in CO hydrogenation. Adapted with permission from Ref[24]. Copyright 2013, Springer Science Business Media New York.

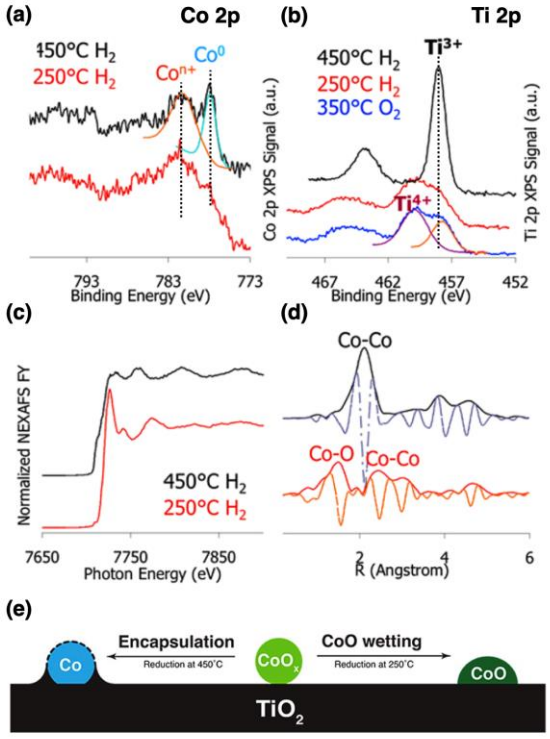

Fig.2 Ambient-Pressure X-ray Photoelectron Spectroscopy (AP-XPS) spectra of the Co/TiO_2 catalyst at (a) Co 2p and (b) Ti 2p core levels under various conditions. (c) Near Edge X-ray absorption fine structure (NEXAFS) spectra and (d) the corresponding Extended X-day Absorption Fine Structure (EXAFS) oscillation at Co K edge at different temperatures. (e) Schematic representation of proposed surface reconstruction under oxidative and reductive environments. Adapted with permission from Ref[25]. Copyright 2014 American Chemical Society.

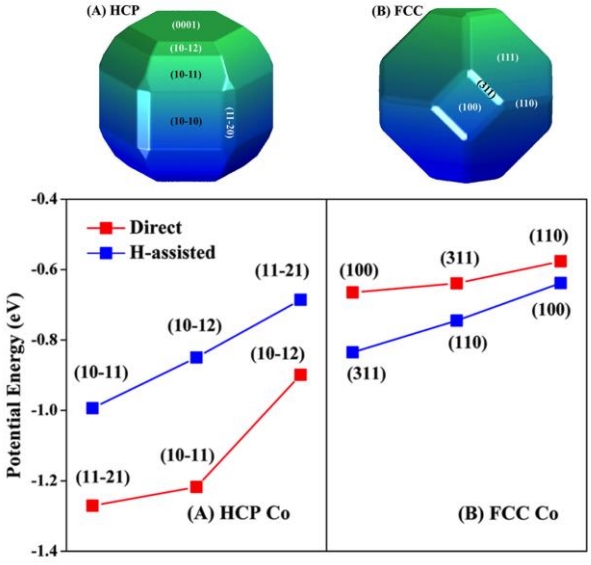

Fig.3 Calculated potential energy (in eV) for CO dissociation at the transition states for C=O breaking via the direct route (red) and the H-assisted route (blue) on (A) HCP Co facets and (B) FCC Co facets. The equilibrium morphology of HCP Co and FCC Co based on the Wulff construction from DFT were presented on top. Adapted with the permission from Ref[79].Copy right 2013 American Chemical Society.

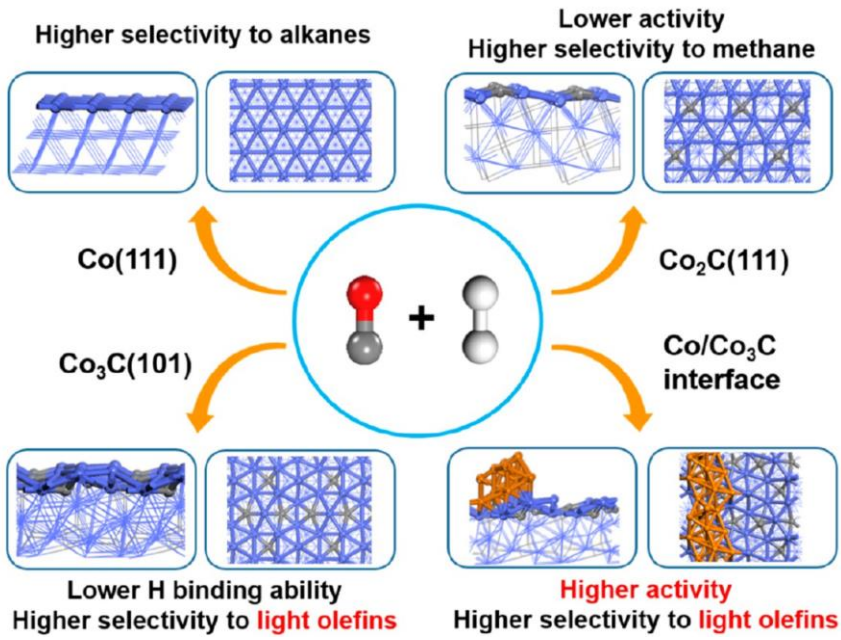

Fig.4 Schematic summary of the selectivity of Co(111), Co_2C (111), Co_3C (101) and Co/Co_3C interface. Adapted with permission from Ref[84]. Copyright 2019 American Chemical Society.

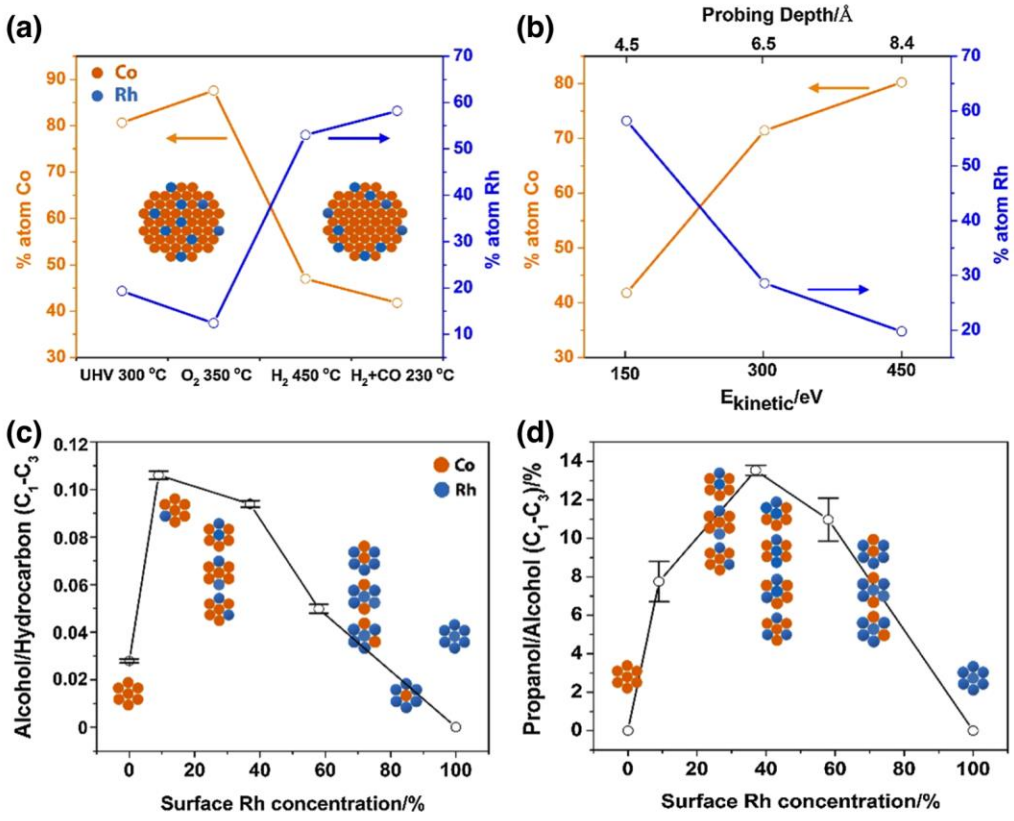

Fig.5 (a) Surface composition and (b) probing depth profile of Co-Rh_10 under various conditions, calculated from AP-XPS data. (c) Alcohols to hydrocarbons ratio and (d) percentage of propanol

in total alcohol product as a function of surface Rh concentrations. Adapted with permission from Ref[26]. Copyright 2016, Springer Science Business Media New York

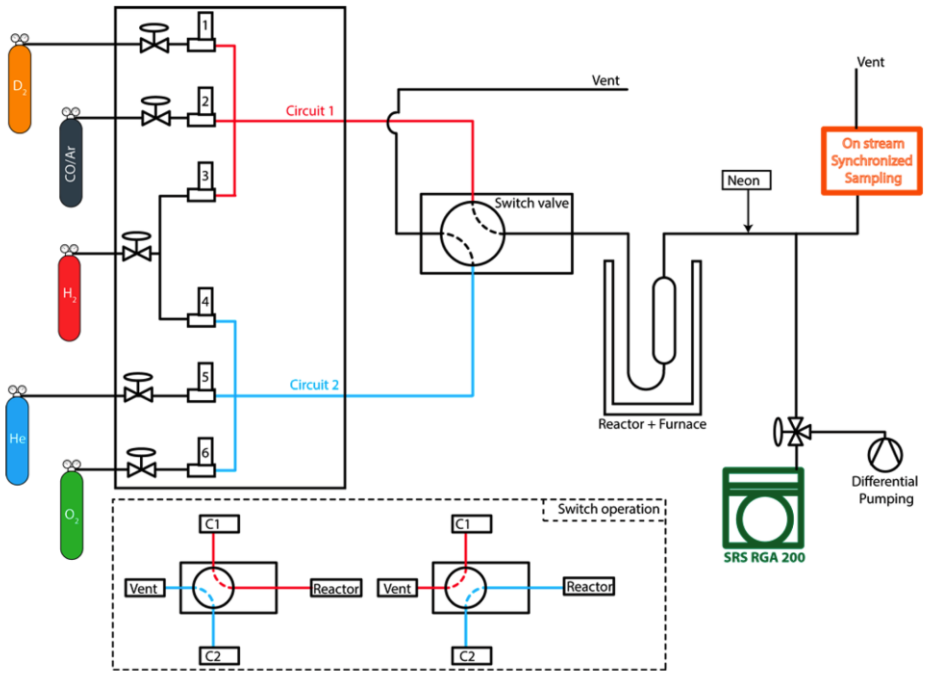

Fig.6 Schematic presentation of the gas-line, reactor and analyzer used for chemical transient kinetic experiments. Inset shows the valve switch to allow the fast gas change from circuit 1 to circuit 2. Adapted with permission from Ref [28]. Copyright 2014 American Chemical Society.

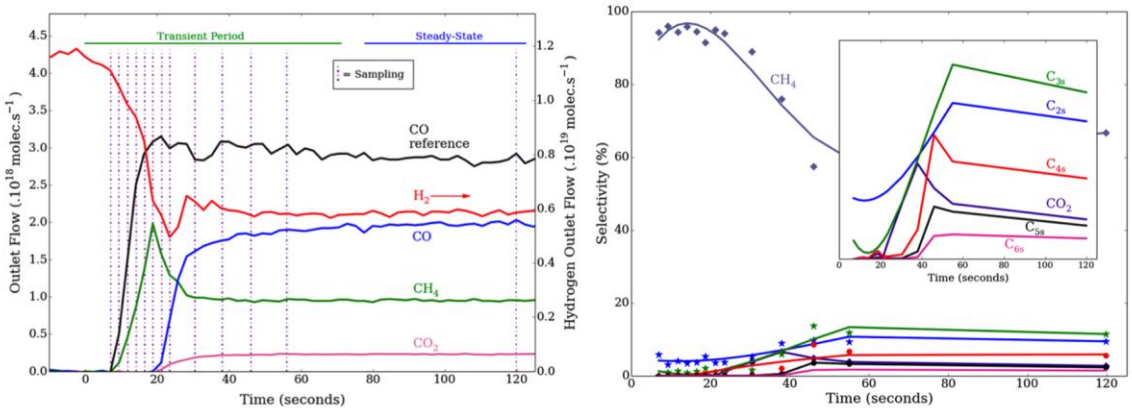

Fig.7 (a) Online QMS data shows the transient period (0~65 s) and steady-state (after 65s). The vertical dashed lines represent the moment when GC-MS samples were collected. (b) Selectivity as a function of time obtained from GC-MS data. The reaction was carried out using CoMgO as the catalyst at 230 ˚C and ambient pressure under H_2 and CO flow (3:1). Inset is the zoom-in region to show the appearance time of different products. Adapted with permission from Ref[28]. Copyright 2014 American Chemical Society.

(1) Carbide Mechanism

Chain Initiation: CO dissociation and hydrogenation

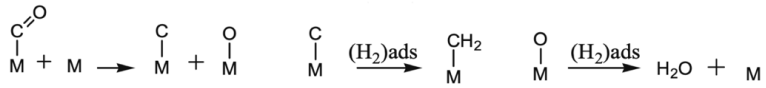

Chain Growth

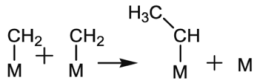

Chain Termination

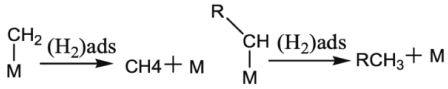

(2) Hydroxycarbene Mechanism

Chain Initiation: formation of hydroxy carbene

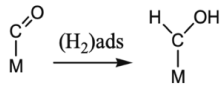

Chain Growth

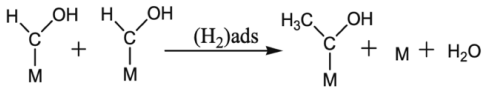

Chain Termination

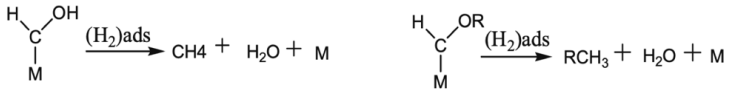

(3) CO Insertion Mechanism

Chain Initiation: reduction of adsorbed CO

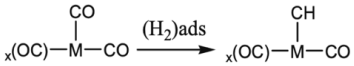

Chain Growth

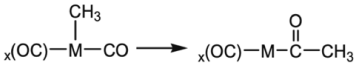

Chain Termination

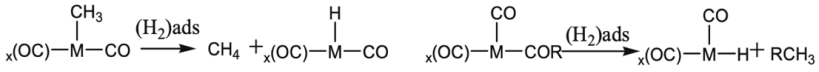

Fig. 8 Three main mechanism of F-T synthesis. Adapted with permission of Ref[95]. Copyright 2014, Springer Nature.

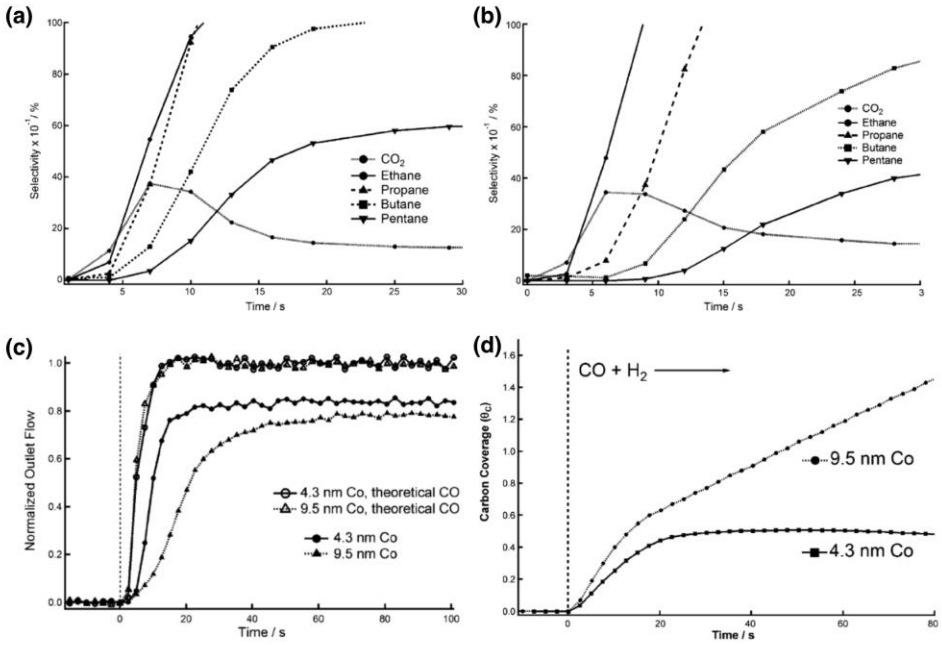

Fig. 9 Carbon selectivity as a function of time of (a) 4.3 nm Co/MCF-17 and (b) 9.5 nm Co/MCF-17. (c) Normalized outlet flow and theoretical flow of CO for 4.3 nm and 9.5 nm CO/MCF-17. (d) Carbon coverage (θ_c) for 9.5 nm and 4.3 nm Co/MCF-17. Adapted with permission from Ref[27]. Copyright 2017 Wiley-VCH Verlag GmbH & Co. KGaA, Weinheim.